

Supporting Information

Reactive Simulations-based Model for the Chemistry behind Condensed Phase Ignition in RDX crystals from Hot Spots

Kaushik L Joshi, Santanu Chaudhuri*

Illinois Applied Research Institute

University of Illinois at Urbana-Champaign, Champaign IL 61820

Comparison between original ReaxFF and ReaxFF-Ig for α -RDX.

Simulation description:

MD-NPT simulations were performed on α -RDX with starting density of 2.26 g/cm^3 . The unit cell dimensions and starting atomic positions were obtained from DFT calculations explained in the main article. Initially, energy minimization was performed on the unit cell to relax atomic positions. After minimization, the unit cell was optimized at set temperature of 300K and set pressure of 5.2 GPa using NPT ensemble. Figure S1 shows the variation of unit cell volume and system pressure as a function of MD steps. Table ST1 compares the optimized system density of original ReaxFF and ReaxFF-Ig at 5.2 GPa with DFT predictions.

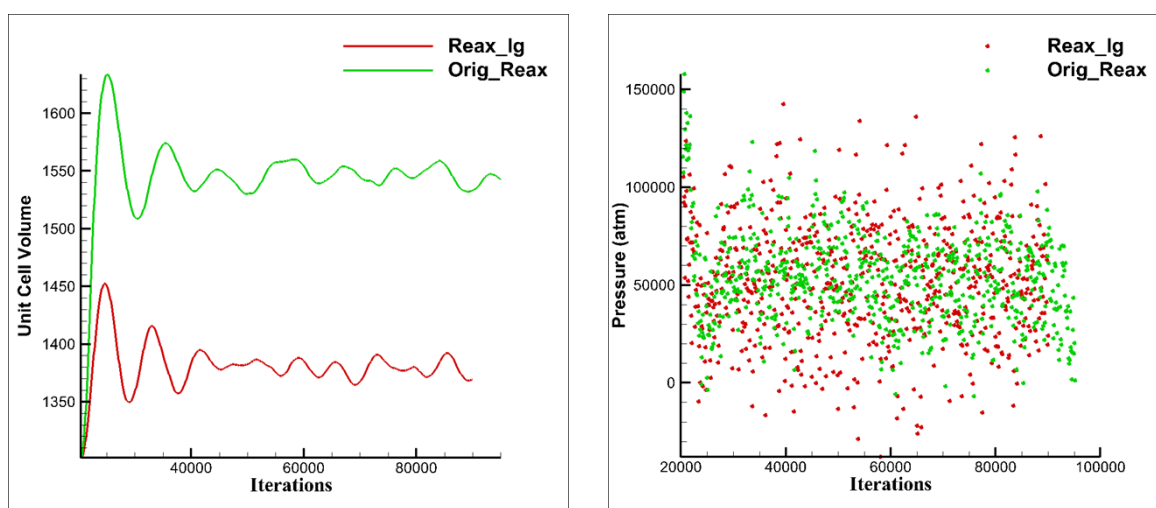


Figure S1: Variation of unit cell volume and system pressure during NPT cell optimization

Table ST1: Optimized density and % error in density by computational methods

	DFT	Original ReaxFF	ReaxFF-Ig
Density (g/cm^3)	2.26	1.89	2.11
% Error in Density	-	16.3%	6.6%

Experimental density was used for the ReaxFF simulations in order to keep the energy density same. The experimental structure was relaxed using DFT-D (dispersion corrected periodic DFT calculations at PBE level) and used in ReaxFF calculated constant volume (NVE) simulations.

DFT calculations on N-N bond Cleavage in γ -RDX

For DFT calculations on N-N bond cleavage, the combined quantum mechanics-interatomic potential functions (QM-Pot) approach was employed to predict decomposition reaction energies of γ -RDX¹⁻⁴. In the QM-Pot approach, as described by Sierka and Sauer⁵, the entire system (S) is partitioned into an inner region (I) and outer region (O). A single γ -RDX crystal unit cell is considered (S) and a selected region within (S) is considered (I). The energy of the whole system is expressed as:

$$E(S)_{high/low} = E(S)_{low} + [E(I)_{high} - E(I)_{low}] \quad (1)$$

In equation (1), the term $E(I)_{high} - E(I)_{low}$ is referred to the correction term. Link atoms are connected to atoms in the inner region in order to complete the chemical bonds and the distance between a link atom and an atom in (I) is defined to be reasonable and at constant value. The positions of link atoms are changed during the optimization process, yet their forces are not taken into account in the optimization algorithm.

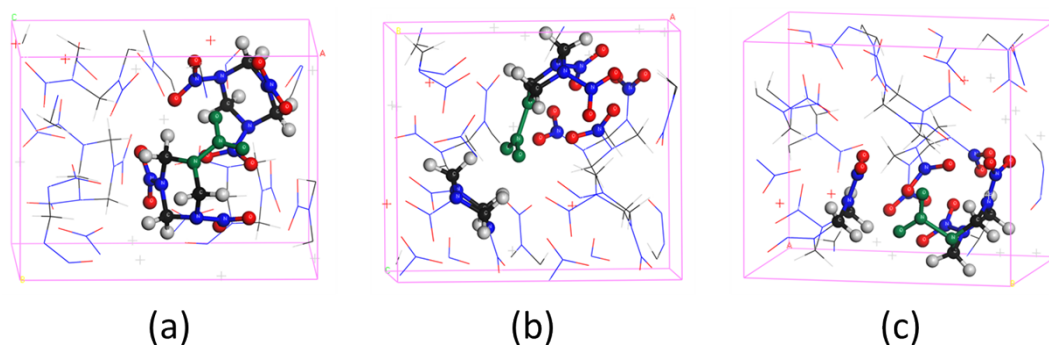
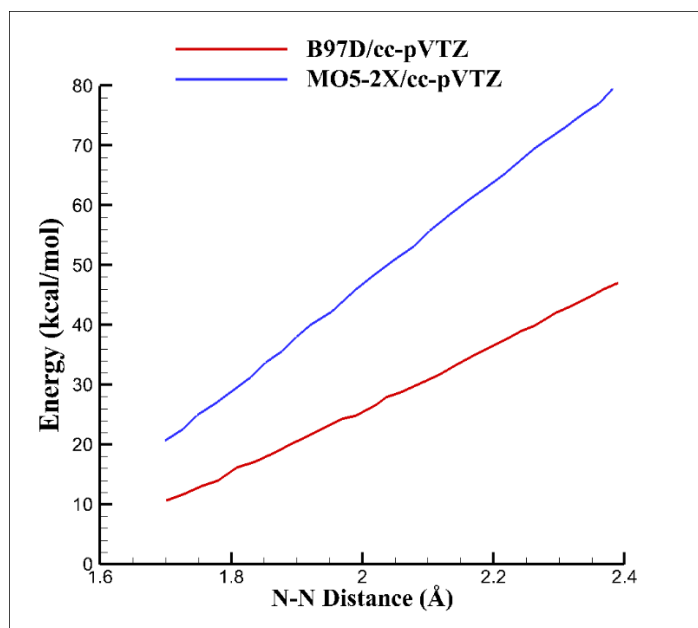


Figure S2: A schematic description of lower and higher level regions in a γ -RDX unit cell optimized using DFT-D method and coupling of regions treated using QMPot approach (Tekarli, S, Le, H., and Chaudhuri S *Manuscript under preparation*). Three different High/Low QM:QM regions are shown to capture the different dissociation barriers for three N-NO₂ bond in one of the triazine ring in the γ -RDX lattice.

Three levels of theory were chosen for the (I) and one for (S) in order to construct the QM:QM hybrid calculations in QM-Pot: second-order Moller-Plesset perturbation method (MP2)⁶, M05-2X⁸, and B97D⁷ for high-level calculations and GGA-PBE was used for low-level calculations. The Gaussian09 program suite was utilized in the high-level calculations⁹. M05-2X and other functionals of the same class were implemented and tested against several traditional DFT methods in a detailed comparison by Zhao et al¹². M05-2X and B97D calculations were performed in conjunction with correlation consistent cc-pVTZ basis set constructed by Dunning et al¹³⁻¹⁷. The calculations show that for high-pressure γ -phase of RDX, the gas-phase barriers increase several tens of kcal/mol. In fact, no true transition state was found for N-N dissociation in a perfect crystal using QM:QM hybrid calculations. The nearest transition state exists for intermolecular concerted H-transfer from adjacent C-H. Similar intramolecular H-transfer is needed to facilitate the formation HNO₂ or HONO (Tekarli, S, Le, H., and Chaudhuri S *Manuscript under preparation*). Thus, the observed suppression of N-NO₂ bond dissociation in ReaxFF is reasonable trend from higher level DFT calculations on DFT-D optimized unit cell (Figure S2). Figure S3 shows the increase in the barrier for N-NO₂ bond dissociation. Such predictions are in line with ReaxFF results described in the manuscript.



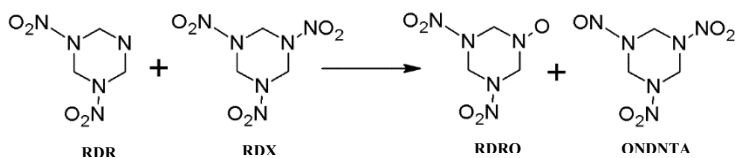
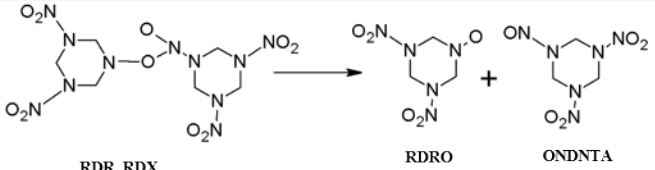
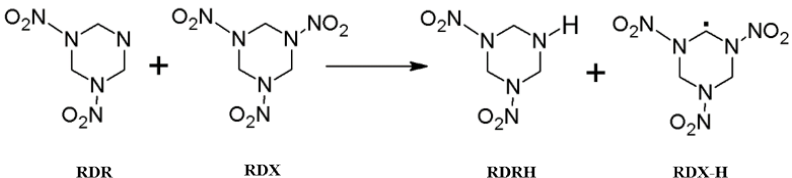
S3. Potential Energy Profile of NO₂ dissociation calculated from QM:QM methods showing no transition state saddle point during the scans using different theoretical methods

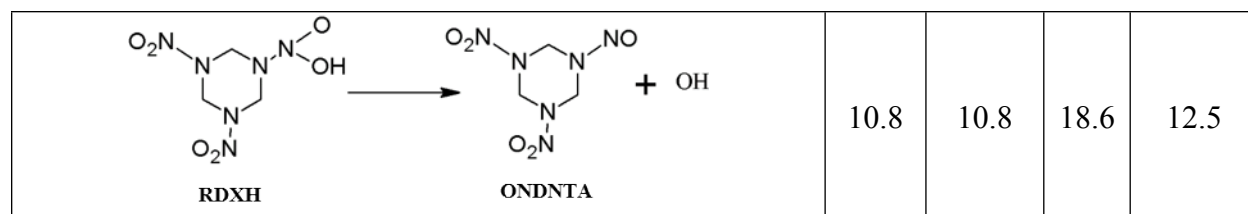
Comparison between DFT and ReaxFF for Chemical Reactions of Intermediates Radicals

The original ReaxFF force field has been trained against extensive training set of CHNO chemistry. For checking the suitability of the force field for our simulations, we have performed additional energy scans for some bimolecular reactions that involve hydrogen and oxygen transfer between intermediate radicals. The DFT reaction enthalpies and activation enthalpies are taken from recent work by Irikura¹⁸. In the DFT work, the author investigated qualitative reactions by using isopotential searching (IPS)¹⁹ on a potential energy surface defined by the semiempirical PM3²⁰ method denoted as IPS//PM3. The subsequent gas-phase properties were computed using density functional theory with the hybrid functional B3LYP²¹⁻²³ and the 6-31G (d) basis sets (Cartesian polarization functions, “6D”). The complete details about DFT calculations can be found in Ref 18.

Since the DFT energies were reported at 298K, we performed the MD-NVT energy scans at 298K for each reaction to obtain an estimate of the reaction enthalpy and activation enthalpy. During each MD run, the temperature is rescaled after every 10 steps. The atoms corresponding to the reaction coordinate were frozen during the MD simulation for each image. For each image, 30,000 MD steps were performed with time step of 0.1fs. The potential energy was averaged over last 3000 time steps to eliminate inherent noise due to thermal fluctuations. Table ST2 compares the ReaxFF activation and reaction enthalpies with the DFT energies for four reactions. It can be seen that the current force field qualitatively reproduces the DFT trend for the gas phase oxygen and hydrogen transfer reactions that the intermediate chemical radicals can undergo during RDX combustion.

Table ST2: Comparison between DFT and ReaxFF for reaction energies of intermediate radicals

Reaction Pathway	DFT ¹⁸ (kcal/mol)		ReaxFF (kcal/mol)	
	ΔE	ΔH	ΔE	ΔH
 <p>RDR + RDX → RDRO + ONDNTA</p>	24.3	-12.9	15.2	-12.1
 <p>RDR + RDX → RDRO + ONDNTA</p>	0	-28.6	4.3	-17.4
 <p>RDR + RDX → RDRH + RDX-H</p>	7.4	-9.5	10.2	-14.2



References:

1. De Moor, B. A.; Reyniers, M. F.; Sierka, M.; Sauer, J.; Marin, G. B. *J. Phys. Chem. C* **2008**, *112*, 11796.
2. Eichler, U.; Kölmel, C. M.; Sauer, J. *J. Comput. Chem.* **1997**, *18*, 463.
3. Tuma, C.; Sauer, J. *Chem. Phys. Lett.* **2004**, *387*, 388.
4. Tuma, C.; Sauer, J. *Phys. Chem. Chem. Phys.* **2006**, *8*, 3955.
5. Sierka, M.; Sauer, J. In *Handbook of Materials Modeling*; Yep, S., Ed.; Springer: Dordrecht, The Netherlands, 2005; Vol. 1, p 241.
6. Møller, C.; Plesset, M. S. *Phys. Rev. B* **1934**, *46*, 618.
7. Grimme, S. *J. Comp. Chem.* **2006**, *27*, 1787.
8. Zhao, Y.; Schultz, N. E.; Truhlar, D. G. *J. Chem. Theory. Comput.* **2006**, *2*, 364.
9. Frisch, M. J.; Trucks, G. W.; Schlegel, H. B.; Scuseria, G. E.; Robb, M. A.; Cheeseman, J. R.; Scalmani, G.; Barone, V.; Mennucci, B.; Petersson, G. A.; Nakatsuji, H.; Caricato, M.; Li, X.; Hratchian, H. P.; Izmaylov, A. F.; Bloino, J.; Zheng, G.; Sonnenberg, J. L.; Hada, M.; Ehara, M.; Toyota, K.; Fukuda, R.; Hasegawa, J.; Ishida, M.; Nakajima, T.; Honda, Y.; Kitao, O.; Nakai, H.; Vreven, T.; Montgomery Jr., J. A.; Peralta, J. E.; Ogliaro, F.; Bearpark, M.; Heyd, J. J.; Brothers, E.; Kudin, K. N.; Staroverov, V. N.; Kobayashi, R.; Normand, J.; Raghavachari, K.; Rendell, A.; Burant, J. C.; Iyengar, S. S.; Tomasi, J.; Cossi, M.; Rega, N.; Millam, N. J.; Klene, M.; Knox, J. E.; Cross, J. B.; Bakken, V.; Adamo, C.; Jaramillo, J.; Gomperts, R.; Stratmann, R. E.; Yazyev, O.; Austin, A. J.; Cammi, R.; Pomelli, C.; Ochterski, J. W.; Martin, R. L.; Morokuma, K.; Zakrzewski, V. G.; Voth, G. A.; Salvador, P.; Dannenberg, J. J.; Dapprich, S.; Daniels, A. D.; Farkas, Ö.; Foresman, J. B.; Ortiz, J. V.; Cioslowski, J.; Fox, D. J.; Revision A.1 ed.; Gaussian, Inc.: Wallingford CT, 2009.
10. Ditchfield, R.; Hehre, W. J.; Pople, J. A. *J. Chem. Phys.* **1971**, *54*, 724.
11. Hehre, W. J.; Ditchfield, R.; Pople, J. A. *J. Chem. Phys.* **1972**, *56*, 2257.
12. Zhao, Y.; Truhlar, D. G. *Acc Chem. Res.* **2008**, *41*, 157.
13. Woon, D. E.; Dunning Jr., T. H. *J. Chem. Phys.* **1993**, *98*, 1358.
14. Kendall, R. A.; Dunning Jr., T. H.; Harrison, R. J. *J. Chem. Phys.* **1992**, *96*, 6796.

15. Dunning Jr., T. H. *J. Chem. Phys.* **1989**, *90*, 1007.
16. Peterson, K. A.; Woon, D. E.; Dunning Jr., T. H. *J. Chem. Phys.* **1994**, *100*, 7410.
17. Wilson, A. K.; Van Mourik, T.; Dunning Jr., T. H. *J. Molec. Struct.* **1996**, *388*, 339.
18. Irikura, K. K.; *J. Phys. Chem. A* 2013, *117*, 2233
19. Irikura, K. K.; Johnson, R. D.; *J. Phys. Chem. A* 2000, *104*, 2191
20. Stewart, J. J. P.; *J. Comput. Chem.* 1989, *10*, 209
21. Becke, A. D.; *J. Chem. Phys.* 1993, *98*, 5648–5652.
22. Stephens, P. J.; Devlin, F. J.; Chabalowski, C. F.; Frisch, M. J. J.; *J. Phys. Chem.* 1994, *98*, 11623.
23. Lee, C.; Yang, W.; Parr, R. G.; *Phys. Rev. B* 1988, *37*, 785